Amphiphilic Janus Magnetoplasmonic Nanoparticles: pH-Triggered Self-Assembly and Fluorescence Modulation

Derong Lu,[†] Shuai Hou,[†] Sheng Liu,[‡] Qirong Xiong,[†] Yonghao Chen,[†] Hongwei Duan*[†]

[†] School of Chemical and Biomedical Engineering, Nanyang Technological University, 70 Nanyang Drive, Singapore 637457.

[‡] Division of Physics and Applied Physics, School of Physical and Mathematical Sciences, Nanyang Technological University, Singapore 637371

Abstract

We report amphiphilicity-driven self-assembly of polymer-coated magnetoplasmonic Janus nanoparticles (JNP) that result in well-defined colloidal ensembles with controllable size, morphology, and dimension. The amphiphilic JNP building blocks were prepared by coating fluorescent dye-conjugated pH-responsive block copolymer (BCP) and hydrophilic polymers on plasmonic and magnetic side of the JNPs, respectively. Our results have demonstrated a direct correlation between the amphiphilicity of the JNP building block and the structural parameters of corresponding ensembles. It was found that the increase of the relative ratio of pH-responsive hydrophobic BCP and hydrophilic polymer grafts on two different parts of the JNP led to the morphological transition of the assemblies from micellar cluster to lamellae to vesicle. It provides insight into the colloidal self-assembly of functional nanocrystal. Furthermore, the coating of well-defined BCP grafts on the gold nanoparticle (AuNP) of the

JNPs offers the possibilities to finely tune the interparticle distance and precisely position dye molecules at the gap between neighboring JNPs in the ensembles, and the pH-sensitivity of the BCP allows to control the interparticle distance as a function of pH. Such dye-encoded magnetoplasmonic ensembles can serve as a well-defined platform to study the metal-fluorophore interaction, tleading to an improved fundamental understanding of metal-enhanced fluorescence (MEF) process. The fluorescent magnetoplasmonic ensembles with defined morphologies (i.e., multimers and vesicles) are of broad interest for biomedical applications that require synergistic multifunctionalies such as theranostics and biosensors.

1. Introduction

Colloidal assemblies formed by plasmonic nanostructures often exhibit distinct physicochemical properties that are not available for their discrete building blocks.[1-3] Considerable efforts have been exerted on developing the assembling method of PNCs, actuated by the collective properties of PNC-derived assemblies.[4] Particularly, amphiphilicity-driven self-assembly of PNC enabled by decorating PNC with amphiphilic polymers has been demonstrated a powerful tool to construct plasmonic assemblies with defined dimension and morphology.[5-10] The main driving force of the self-assembly of polymer-PNC building block is the hydrophobic interaction between polymer grafts and dispersing media.[11] Moreover, responsive polymers as surface ligands make it possible to continuously tune inter-PNCs distances by corresponding external stimuli. Note that most of PNC-polymer building blocks used for the colloidal self-assembly are symmetric in terms of surface chemistry. That is, the surface of PNCs is evenly coated with either mixed hydrophobic and hydrophilic polymers or

with amphiphilic BCPs.[2] Such PNC-polymer hybrid building blocks are inherently distinct with asymmetric BCPs that consisting of well-separated hydrophobic and hydrophilic blocks. To achieve a higher level control of the structural details of resulting assemblies, a well-defined asymmetric PNC-polymer hybrid building block that is a colloidal analogue of amphiphilic BCP, is necessary.

In the polymer-assisted assemblies, the PNC building blocks would be closely packed with the formation of tight junctions (nanogaps) between neighboring PNCs.[8, 12, 13] A localized and significantly enhanced electromagnetic filed inside the gap region form the "hot-spot" resulting from the strong plasmonic coupling of pairing PNCs.[14, 15] Fluorescence dyes located in the "hot-spot" can experience an augmented excitation light intensity and thus exhibit a dramatically amplified optical signal due to an antenna effect.[16, 17] This structural characteristic makes plasmonic assemblies an intriguing platform to investigate plasmon-molecule interaction,[18, 19] such as metal-enhanced fluorescence (MEF),[17, 20] which can further endow light-mediated applications for bioimaging, biosensing, and nanomedicine.[21]

For a fluorescent dye locating in a proximity of PNC (*e.g.,* AuNP) surface, its apparent fluorescence emission intensity is manipulated by a synergistic effect of excitation enhancement, surface quenching, and plasmon modulation of overall quantum yield (QY).[22] The first factor is sensitive to inter-PNC distance and relative physical position of dye to the electric field. Placing dye molecules in a PNC coupling-induced enhanced electric field can lead to an increased excitation rate of dye, thus giving rise to fluorescence enhancement.[20, 23] The second factor is primarily depended on the separating distance (d) between dye and PNC. When the dye is absorbed on or is in close proximity (e.g., $d < 5$ nm) to PNC surface, energy

transfer from the dye to PNC will cause fluorescence quenching due to the increase of the nonradiative decay rate.[24, 25] The overall QY, in the case of dye-encoded plasmonic assemblies, is determined by both intrinsic QY of dye and the scattering-to-absorption ratio (Scat/(Scat+Abs)) of the PNC assembly, because the emission process of dyes can be coupled to the far field through the scattering of PNC-based ensembles.[22] Moreover, the scattering intensity dominates the extinction upon the formation of large-sized assemblies, giving an increased Scat/(Scat+Abs) ratio of the PNC assemblies compared to individual building blocks, which is beneficial to improving the overall QY.[20] Collectively, positioning dyes within the nanogaps of PNC assemblies, controlling dye-PNC and interparticle distances at a nanometer precision , and the size and morphology of assemblies hold the key to achieve tailored plasmon-molecule interaction.[26]

Here we investigate how structural parameters of JNP building block and pH of dispersing media affect the apparent fluorescence emission intensity of dye-encoded plasmonic assemblies. Well-defined polymer-coated magnetoplasmonic JNPs (Au/$MnFe_2O_4$, Au/MFO) was synthesized (Figure 1), in which the plasmonic (*i.e.,* AuNP) and magnetic part (i.e., $MnFe_2O_4$) were coated with pH-responsive hydrophobic BCP with covalently conjugated cyanine 3 (Cy3) dyes and hydrophilic polymers, respectively. The resulting JNP with asymmetric composition and surface chemistry imparted pH-triggered amphiphilicity-driven self-assembly to produce a series of assemblies in aqueous solution. A morphological transition from cluster to lamellae to vesicle was realized by adjusting the relative ratio of hydrophobic BCP and hydrophilic grafts. Notably, the design of BCP attached on the AuNPs ensure the Cy3 locating at the center of the gaps between neighbouring AuNPs, leading to precise control of

the PNC-dye distance. Moreover, the Cy3-conjugated pH-sensitive BCP grafted on the AuNP acted as a responsive modulator to control the assembly/disassembly of assemblies and tune the interparticle and Cy3-AuNP distances inside the assemblies as a function of pH. The combination of experimental results and theoretical simulation revealed the contribution of different factors to the QY of assemblies, which is conducive to achieving an in-depth understanding of the MEF process. Also important is that integrating both plasmonic and magnetic components into a single JNP provides the possibility for producing well-defined multifunctional assemblies, which hold promise in multi-modality applications based on enhanced fluorescent signal and magnetoplasmonic properties of the assemblies.

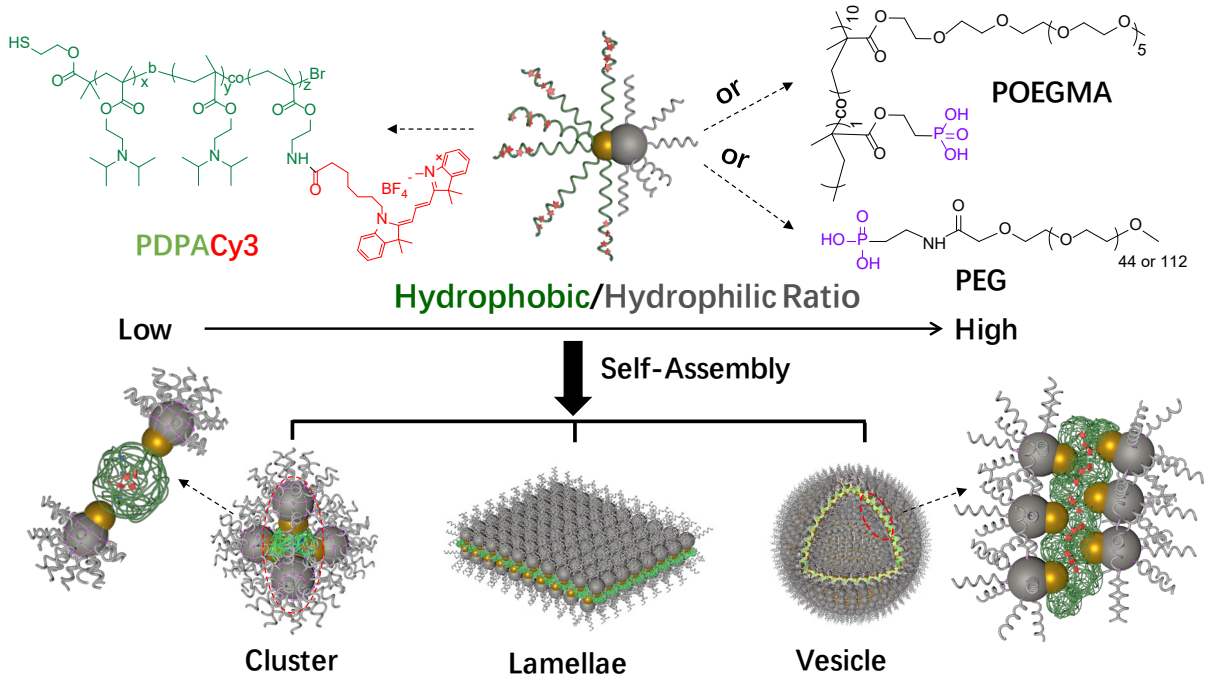

Figure 1: Schematic illustration of ensembles constructed by the self-assembly of amphiphilic JNPs with different hydrophobic/hydrophilic ratio of polymer grafts.

2 Results and Discussion

The Au/MFO JNP was prepared by growing the MFO part on the surface of Au seeds.[27, 28] The average diameter of AuNP is ~9 ± 0.8 nm determined by transmission electron microscopy (TEM, Figure S1). Amphiphilic Au/MFO nanoparticles (NPs) were prepared through a "grafting onto" strategy, by which the pre-synthesized hydrophilic polymers and dye-containing pH-responsive BCPs were sequentially conjugated onto the JNP through ligand exchange reactions (Figure 1). In brief, Au/MFO JNPs were first decorated by phosphonic acid-functionalized Poly(oligo(ethylene glycol) methyl ether methacrylate (POEGMA) or poly(ethylene glycol) (PEG, with 112 or 44 repeating units), giving rise to Au/MFO-POEGMA, Au/MFO-PEG_{112}, and Au/MFO-PEG_{44}, respectively (Figure 1 and Table 1). The synthetic details and NMR characterizations of phosphonic acid-functionalized POEGMA and PEG are available in the supporting information (SI, Scheme S1 and S2, and Figure S3-S9). Of note is that using POEGMA bearing multiple anchoring groups (*i.e.,* phosphonic acid) to modify Au/MFO afforded a higher content of hydrophilic grafts (*i.e.,* 17wt%) for Au/MFO-POEGMA, compared to that of Au/MFO-PEG_{112} and Au/MFO-PEG_{44} with a hydrophilic content of 13% and 8%, respectively, determined by thermogravimetric analysis (TGA, Figure S10A, Table S1).

Recent advance in living radical polymerizations such as atom transfer radical polymerization (ATRP) has offered a feasibility to synthesize well-defined dye-conjugated stimulus-responsive BCPs with controlled composition and architecture (Scheme S3).[29, 30] To modify the Au part of JNP, a series of thiol-terminated, Cy3-conjugated and pH-responsive BCPs (Figure 1), consisting of a poly 2-(diisopropylamino)ethyl methacrylate (PDPA) block

and a PDPA-*co*-poly(2-aminoethyl methacrylate) (PAMA)-Cy3 random copolymer segment, were synthesized through ATRP (Scheme S3, Table S2, and S3). During the ATRP, a homo-PDPA block was prepared first and acted as a macroinitiator to initiate both DPA and AMA monomers to afford a second segment of a PDPA-*co*-PAMA random copolymer (Scheme S3). Cy3 dyes were future conjugated to amine groups of the AMA units, followed by a reducing step to yield thiolated block copolymers (PDPACy3, Table 1). The amount of conjugated dye was predetermined by controlling the degree of polymerization of AMA monomer. The DPA units in the second block can act as a spacer to separate the adjacent Cy3 to minimize the self-quenching effect. The results of ^{1}H NMR and SEC characterizations (*i.e.,*) of resulting PDPACy3 block copolymers and corresponding precursors are summarized in Figure S11-S12, Table S2 and S3. Notably, the intrinsic QY of the Cy3 dyes in thePDPACy3 copolymers in different solvents (*i.e.,* DMF, pH 8.5 and pH 4 aqueous solutions) were very close to that (0.19) of free Cy3 dye in DMF (Figure S13). The similar QYs in different solvents suggested that the self-quenching between the neighboring Cy3 dyes on the copolymer backbone was negligible, as a result of the separating effect offered by DPA monomeric units (15~17 units in average, Table S3).[31] Subsequent anchoring of PDPACy3 copolymers of different molecular weight (M_w) and composition on Au/MFO-POEGMA, Au/MFO-PEG$_{112}$, and Au/MFO-PEG$_{44}$ led to amphiphilic JNPs (*i.e.,* JNP1-JNP4 listed in Table 1 and S1) with varied ratio of hydrophobic and hydrophilic polymers grafted on JNP, as determined by TGA (Figure S10B). Herein, the amphiphilic JNPs can be considered as asymmetric amphiphilic colloidal analogues that resemble AB-type amphiphilic di-block copolymers due to the well segregated hydrophobic and hydrophilic polymer grafts on the JNPs.[32]

Table 1: Composition of amphiphilic Au/MFO JNPs and morphologies of corresponding assemblies

Entry	Composition[a]	Ratio[b]	Morphology
JNP1	$PDPA_{48}$-*b*-($PDPA_{18}$-*co*-PAMA/$Cy3_{1.2}$)-Au/MFO-POEGMA	0.76	Cluster
JNP2	$PDPA_{76}$-*b*-($PDPA_{21}$-*co*-PAMA/$Cy3_{1.4}$)-Au/MFO-PEG_{112}	1.69	Lamellae
JNP3	$PDPA_{106}$-*b*-($PDPA_{29}$-*co*-PAMA/$Cy3_{1.7}$)-Au/MFO-PEG_{112}	2.08	Vesicle
JNP4	$PDPA_{106}$-*b*-($PDPA_{29}$-*co*-PAMA/$Cy3_{1.7}$)-Au/MFO-PEG_{44}	3.12	Precipitate

a Determined by SEC, ^{1}H NMR., and UV-vis calculation. The BCPs SH-$PDPA_{48}$-*b*-($PDPA_{18}$-*co*-PAMA/$Cy3_{1.2}$), SH-$PDPA_{76}$-*b*-($PDPA_{21}$-*co*-PAMA/$Cy3_{1.4}$), and SH-$PDPA_{106}$-*b*-($PDPA_{29}$-*co*-PAMA/$Cy3_{1.7}$) refer to PDPACy3-I, PDPACy3-II, and PDPACy3-III, respectively.
b Amphiphilic ratio, refers to the mass ratio of hydrophobic to hydrophilic grafts, determined by TGA analysis.

The pH-triggered self-assembly was conducted by slowly adding pH 8.5 NaOH solution into the DMF solution of JNPs, followed by the dialysis to remove the organic solvent. PDAPA has a pKa of *ca.*5.8 and undergoes hydrophilic to hydrophobic transition at pH 8.5. Interestingly, the morphology of assemblies formed was directly correlated to the mass ratio of hydrophobic and hydrophilic polymers (termed as amphiphilic ratio, Table 1 and S1) attached on the JNPs. By increasing the amphiphilic ratio of JNPs from 0.76 to 2.08, the structural transition of cluster-lamellae-vesicle was observed for the assemblies (Figure 2, Table 1). A relatively low amphiphilic ratio of 0.76 of JNP1 favored the formation of multimer clusters (Figure 2a), among which the tetramer was the dominant species. It could be attributed the dense coating of POEGMA on MFO, which created considerable steric hindrance for incoming JNPs after the formation of cluster, preventing the generation of larger assemblies.

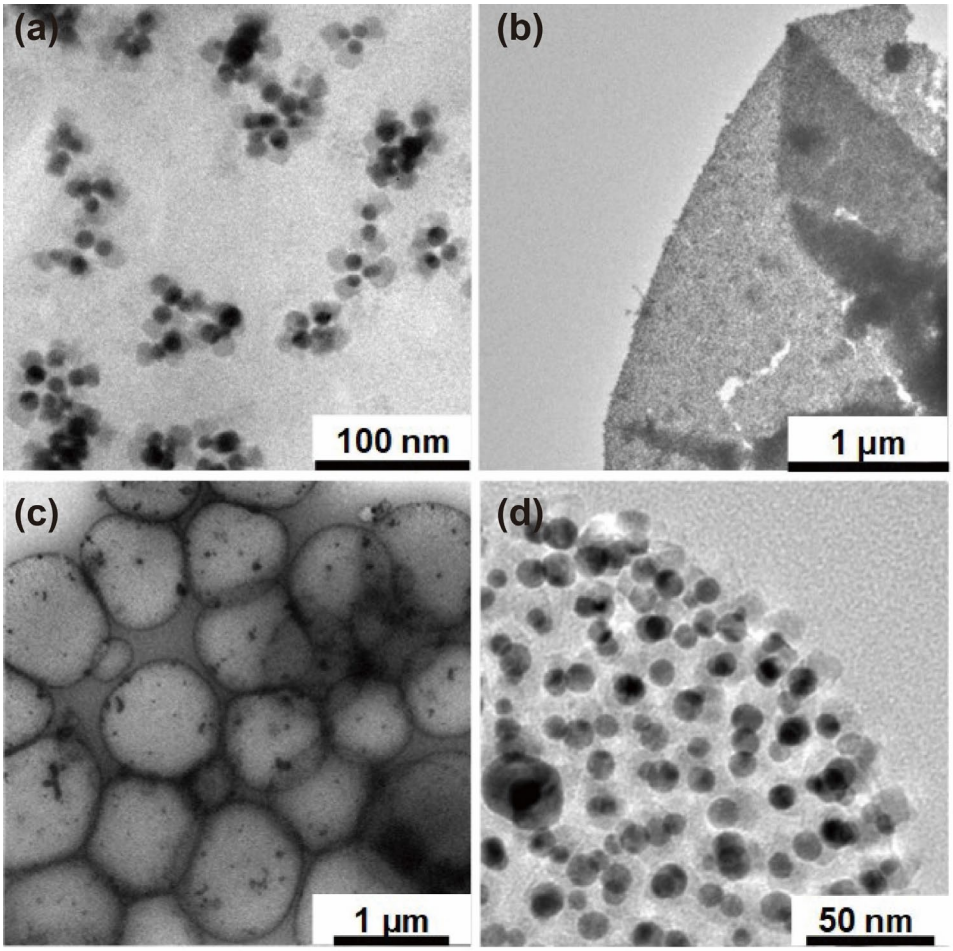

Figure 2: TEM images of ensembles of amphiphilic Au/MFO in pH 8.5 NaOH solution: (a) Cluster, (b) Lamellae, (c) Vesicle, and (d) Edge of vesicle.

The TEM observation of clusters clearly shows that the AuNPs modified by hydrophobic PDPA were headed inside, while the MFOs faced outside owing to the coating of hydrophilic POEGMA (Figure 2a), analogous to the self-assembly of amphiphilic BCPs to form core-shell micelles. The morphology of assemblies derived from JNP2 (with an intermediate amphiphilic ratio of 1.69) transformed to micrometer-scale sheet-like lamellar structures (Figure 2b). Note that the reported examples of two-dimensional (2D) layer of inorganic nanoparticles (INPs) in aqueous solutions are rare. Most polymer-assisted INP 2D arrays were generated in oil/water biphasic condition.[5] JNP3 with a relatively high amphiphilic ratio (*i.e.,* 2.08) preferentiallyformed well-defined vesicular structures, confirmed by both TEM (Figure 2c)

and scanning electron microscopy (SEM) (Figure S14). Because of the heterogeneous and Janus nature of building block, the membrane wall of the JNP3-derived vesicle was similar to that of the polymersome derived from amphiphilic copolymer.[33] TEM image at a higher magnification (Figure 2d) further revealed that the arrangement of the JNP-based vesicle shell showed the co-existence of bilayer and interdigitated structures, which could be attributed to the size mismatch of AuNP and MFO. Furthermore, JNP4 with the highest amphiphilic ratio (*i.e.,* 3.12) only produced a large scale of precipitate (Figure S15), presumably due to the insufficient hydrophilic content on MFO to stabilize the corresponding assembled structure and both Au and MFO moieties are originally coated by hydrophobic ligands. The morphological change of JNP-based assemblies resulted from increasing M_w of PDPA copolymer (from 12.5 to 26.1 KDa) was analogous to the structural transition that occurred in the self-assembly of the amphiphilic BCPs when the weight ratio of hydrophobic block increased.[34]

In addition to acting as a morphology modulator, the well-defined ATRP-generated BCPs also enabled a precise control over the physical position of encoded dyes within the formed nanogaps of the resulting assemblies. For the thiol-terminated PDPACy3, the longer homo-PDPA segment was tethered onto AuNP and distance the shorter Cy3-tagged random block from the AuNP surface. It offers an opportunity to tune the Cy3-AuNP distance by varying the M_w of first PDPA block[35] In the assemblies, the mobility of PDPA chain was greatly decreased due to hydrophobicity-induced aggregation in basic aqueous solution, which restricted the migration of Cy3 molecules inside the assemblies. Therefore, the spacing and immobilizing effects offered by the PDPACy3 grafts ensured that the physical position of Cy3 was primarily restricted at the center of the gap region between the AuNPs (Figure 1). This structural feature

in combination with the tunable Cy3-AuNP distance providing flexibility and feasibility to the dependance of the quenching and excitation enhancement on the Cy3-AuNP distance accordingly. Moreover, pH-sensitivity of the BCP grafts imparted a continuous tuning of the Cy3-AuNP distance in response to the change of pH. These characteristics made Cy3-encoded JNP-based assemblies an ideal platform to investigate the metal-fluorophore interaction. To this end, cluster and vesicle of defined structures were selected to study the experimental and theoretical fluorescence emission process of the encoded Cy3 molecules.

It is well known that the decrease of pH would lead to the protonation of tertiary amine units of DPA and result in the swelling of PDPA due to charge repulsion.[36] As such, the interparticle distance of the assemblies would increase in response to decreasing pH, but the morphology of cluster and vesicle could be maintained if the pH (*e.g.,* pH 8.5 and 6) higher than the p*K*a (*ca.* 5.8~6.2, depending on M_w and grafting density) of PDPA (Figure 3). Further decrease of the pH, *i.e.,* below its p*K*a endows a hydrophobic-to-hydrophilic transition of the PDPACy3 BCPs and trigger the dissociation of the assemblies. For instance, the clusters and vesicles disintegrated into single JNPs (Figure 3c) and small clusters (Figure 3f) at pH 4, respectively.

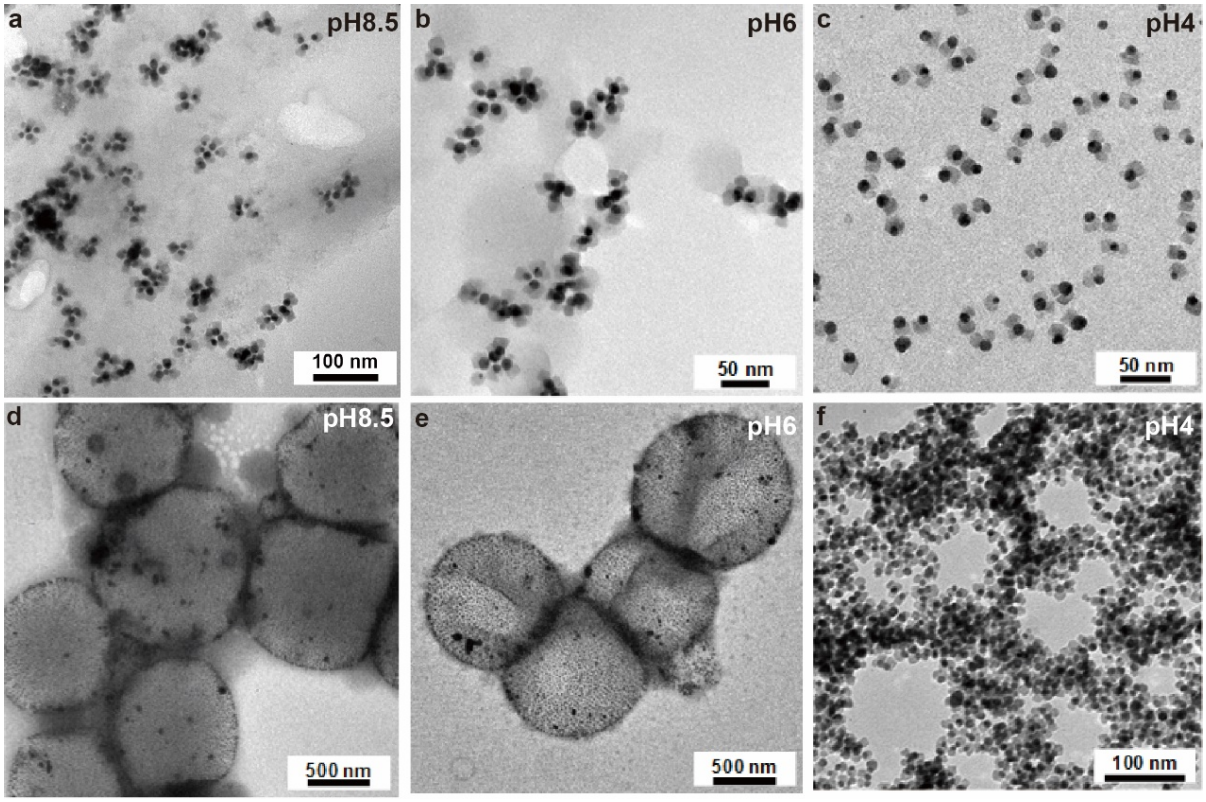

Figure 3: TEM images of the cluster (a-c) and vesicle (d-f) in aqueous solution with different pH.

The variation of dimension and solubility of PDPACy3 grafts directly caused the assembly/disassembly processes and changes in interparticle and Cy3-AuNP distances. Consequently, it is feasible to tailor the apparent fluorescence intensity of Cy3-encoded cluster and vesicle by adjusting the pH of dispersing media. The distance-dependent interparticle plasmonic coupling strongly affected the surface plasmon resonance (SPR) of plasmonic ensembles.[37] The UV-vis spectra of JNP-based assemblies could serve as an indicator of interparticle distances (gap size), which was inherently determined by the dimension of PDPACy3 spacer attached on the AuNP. Upon self-assembly, the SPR of the clusters showed 18 nm red-shifts (at pH 8.5, Figure 4a) relative to that (550 nm) of their discrete units (*i.e.,* JNP1 building block) in DMF. The decrease of pH from pH 8.5 to 6 led to an increased

interparticle distance, resulting in slight blue shifts of SPRs (Figure 4a). The disassembly of clusters from pH 6 onwards, for instance, from pH 6 to 5, gave rise to a sudden blue-shift and continuously shifted to lower wavelength region from pH 5 to 4. On the other hand, the pH variation-induced dimensional change of first block (PDPA homopolymer segment) of the PDPACy3 BCP would directly affect the Cy3-AuNP distance and thus led to the change of the fluorescence intensity of clusters as a function of pH (Figure 4b). At pH 8.5, the normalized fluorescence intensity of clusters experienced a ~50% decay compared to that of JNP1 precursor in DMF (Figure 4c). Further decrease of the pH resulted in a steady increase of enhancement ratio (fluorescence emission intensity of assemblies compared to that of JNP building blocks) and reached a maximal value at pH 4 by a factor of 1.34. Additionally, the lifetime of a dye molecule nearby the AuNP surface is also distance-sensitive[38, 39] A lower pH is associated with a more extended Cy3-AuNP distance, leading to a reduced radiative rate of dye and thus a longer lifetime of dye molecule nearby AuNP. In the case of cluster, the variation of fluorescence lifetime steadily increased as the decrease of pH, exhibiting a same trend as that of fluorescence enhancement ratio but was different from the spectral shift of the SPR peaks (Figure 4c and S16).

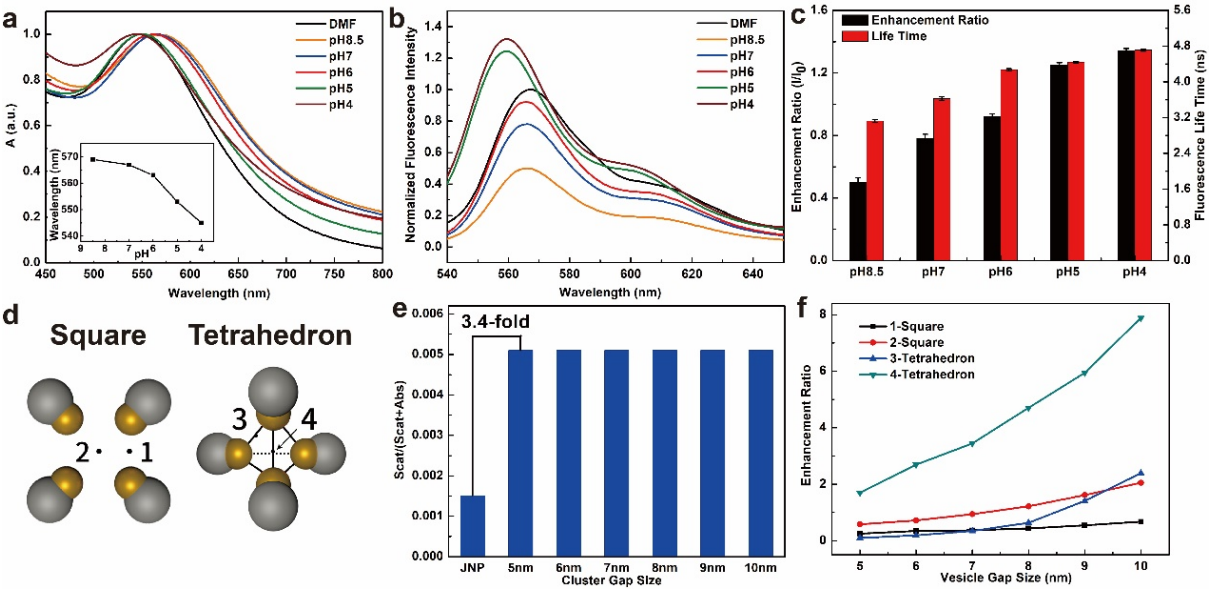

Figure 4: (a) UV-vis spectra of JNP1 before self-assembly (in DMF) and clusters as a function of pH. (Inset: LSPR peak wavelength of clusters). (b) Fluorescence emission intensity spectra of JNP1 (in DMF) and clusters as a function of pH. The intensity of JNP1 in DMF was normalized to 1. (c) Fluorescence intensity enhancement ratio of cluster compared to JNP1 (intensity refer to I and I_0, respectively) and corresponding fluorescence life time of encoded Cy3 as a function of pH. The error bars represent standard deviations (n=3). (d) Cartoon illustrations of possible spatial structures of cluster. 1, 2, 3, and 4 refer to the four positions of Cy3 in the cluster used for simulation. (e) Comparison of the scattering-to-absorption ratio of JNP1 and cluster based on simulation. (f) Simulation of fluorescence enhancement ratio at different positions in clusters by comparing the intensity of cluster and JNP1, the intensity of JNP1 was normalized to 1.

Polymers that are conjugated on INP by the "grafting to" method tend to exist as a coil conformation on the surface of INP due to the relatively low grafting density,[12] behaving as random coils similar to the free polymer in diluted condition in a good solvent.[40, 41] The hydrodynamic diameter (D_h) of the BCP spacer in a good solvent can be determined by the results of size exclusion chromatography (SEC).[42] The D_h of PDPACy3 in pH 4 solution referred to the theoretical maximum Cy3-AuNP distance (see SI for the details of calculation, Table S2, and Equation S7). Moreover, a ~2.3-fold volume shrinkage would occur for the PDPA grafts on the AuNP surface when the solution pH rises above its p*K*a,[36] allowing for estimating

(*e.g.,* $D_{h,pH\ 4}$/2.3) the minimum size of the PDPA-filled nanogap. Based on the $D_{h,SEC}$ and the shrinking ratio, the theoretical gap sizes of the cluster and vesicle are in the range of 4.7-10.8 nm and 7.2 -16.6 nm, respectively (Table S3). It provided a distance reference for the electric profiles and the finite-element method (FEM) simulations.

In case of the clusters, two possible topologies, square and tetrahedron structures, were first selected as models of the JNP arrangement for simulation (Figure 4d). Due to the confinement of Cy3 molecules in the gap area, four representative locations (*i.e.*, 1, 2, 3, and 4, Figure 4d) within the clusters were chosen to calculate the theoretical fluorescent intensity of the Cy3-encoded clusters. It is worth noting that, based on the electric profiles of the clusters (Figure S17), if the encoding Cy3 was located in the central region of the gap, the excitation enhancement of fluorescence derived from the enhanced electric field was almost negligible (that is an enhanced factor of ~1.0), except for the square-type cluster at pH 8.5. It can be ascribed to the presence of a thick PDPA layer and a relatively small size of AuNP (~9 nm). Here a relatively small AuNP (~9 nm) on Au/MFO JNPs led to a short-range enhancement of the electric field away from the surface of AuNP of the corresponding assemblies.[43] Consequently, resulting from the spacing effect endowed by PDPA, in most of the situation (for both clusters and vesicles), the apparent fluorescence intensity was only determined by a combined effect of intrinsic QY of PDPACy3, quenching effect, and the Scat/(Scat+Abs) ratio of assemblies.[44] It should also be pointed out that the assembled clusters exhibited increased physical size compared to monomeric JNPs, theoretically giving rise to an increased Scat/(Scat+Abs) ratio with a factor of 3.4 (Figure 4e). Moreover, the simulation also revealed that the Scat/(Scat+Abs) ratio was mainly determined by the cross section (related to the

physical size) of assemblies but insensitive with the change of gap size.[45] Consequently, the Scat/(Scat+Abs) ratio could be recognized as a relatively constant parameter from pH 8.5 to 6 due to the preservation of the morphology for clusters.

The simulation results provided a theoretical basis to address the evolution of the fluorescence intensity of clusters in response to pH changes. The significant decay in fluorescence intensity of clusters at pH 8.5 (Figure 4b and 4c) can be attributed to a higher quenching efficiency in the assembly, in which the JNP1 building block gave rise to a closer Cy3-AuNP distance. Such a significant decay indicated that the fluorescence enhancement derived from a slight increase (3.4-fold) in Scat/(Scat+Abs) ratio was not enough to compensate the attenuation caused by quenching effect. It could also explain that even though the cluster was disassembled into single JNP at pH 4 (Figure 3c), a state without the scattering-induced enhancement but less quenching effect, an enhanced factor (1.34) was still obtained. The decrease of pH from 8.5 to 4 led to a continuous swelling of PDPA spacer associated with an extending Cy3-AuNP distance. As a result, the fluorescence enhancement ratio increased steadily from pH 8.5 to 4 due to a decreasing quenching effect. The variation of fluorescence enhancement ratio indicated that surface quenching is the dominant effect in the clusters. A factor of 1.34 also suggested Cy3-AuNP distance in pH 4 is larger than that in DMF, as a fact that the D_h of PDPA copolymer in pH 4 solution is larger than that of in DMF (Table S2). Based on the simulation, for the cluster with the gap size from 4.7 to 10.8 nm, all 1, 2, and 3 positions show the enhancement ratio of less than 2. The only exception is position 4, where the Cy3 was in the geometric center of the tetrahedron-like cluster. The comparison of experimental and theoretical results indicated that the cluster had more chances to take the geometry of

tetrahedron than the square geometry and the region close to position 3 and 4 is a most likely position of Cy3 molecules (Figure 4f).

The UV-vis spectra of vesicles (Figure 5a) showed a similar evolution as that of the clusters but with a larger red-shifts (42 nm) at pH 8.5, due to the presence of more plasmonic AuNPs in close proximity. The M_w of the PDPA spacer (*i.e.,* PDPACy3-III) for the vesicle was 2.1 times larger than that of PDPACy3-I used in the case of cluster (Table S3). Vesicle would thus exhibit a distinct fluorescence evolution in response to the change of pH (Figure 5b), due to a broader adjustable range of the gap size and thus a lower quenching efficiency. An enhanced fluorescence intensity was obtained at the pH above p*K*a, with an enhancement ratio of 5 and 6 at pH 8.5 and 6, respectively (Figure 5c). However, the ratios dropped from pH 6 onwards (3.5-fold at pH 5 and 1.4-fold at pH 4). The lifetime of Cy3 encoded in vesicle showed an increasing trend as the increase of pH but exhibited higher values compared to that of in clusters due to the utilization of thicker spacer PDPACy3-III (Figure 5c and S18).

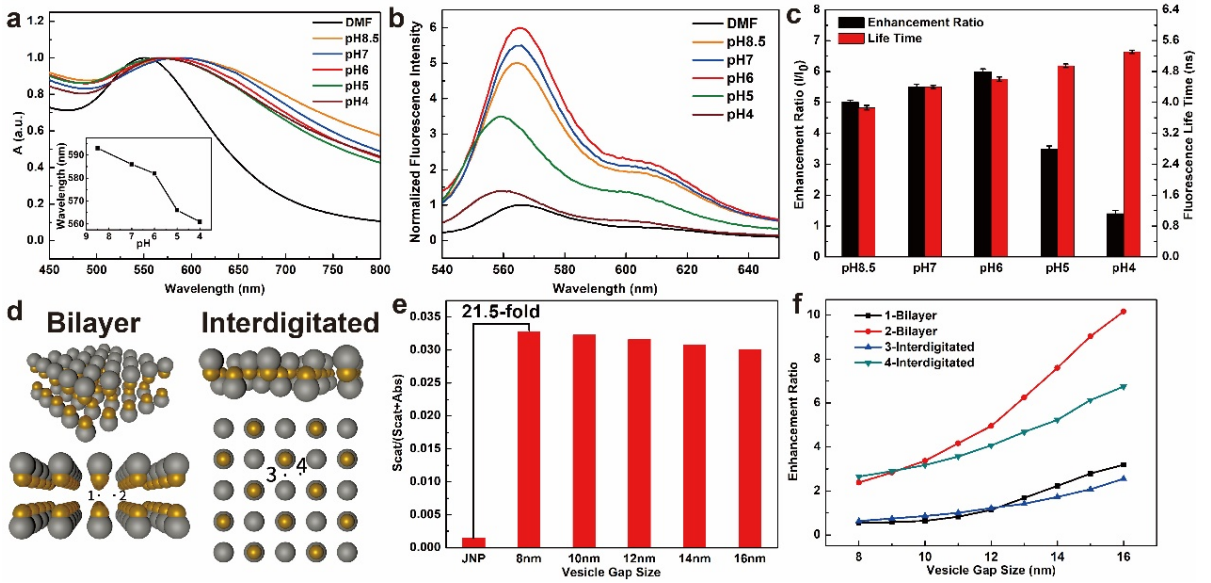

Figure 5: (a) UV-vis spectra of JNP3 before self-assembly (in DMF) and vesicles as a function of pH. (Inset: LSPR peak wavelength of vesicles). (b) Fluorescence emission intensity spectra of JNP1 (in DMF) and vesicles as a function of pH. The intensity of JNP in DMF was normalized to 1. (c) Fluorescence intensity enhancement ratio of vesicles compared to JNP3 in DMF (intensity refer to I and I_0, respectively) and the corresponding fluorescence lifetime of encoded Cy3 as a function of pH. The error bars represent standard deviations (n = 3). (d) Cartoon illustrations of possible spatial layouts of the vesicle membrane. 1, 2, 3, and 4 refer to the four positions of Cy3 in the vesicles used for simulation. (e) Comparison of the scattering-to-absorption ratio of JNP3 and vesicle based on simulation. (f) Simulation of fluorescence enhancement ratio at different positions in vesicle by comparing the intensity of vesicle and JNP3, the intensity of JNP3 was normalized to 1.

According to the TEM images of vesicle wall (Figure 2d), four representative positions (1, 2, 3, and 4) in the central region of the nanogaps were chosen in the bilayer and interdigitated layouts for the simulation (Figure 5d). Vesicle assembled from small JNP3 gave rise to a dramatically increased cross-section and interparticle plasmonic coupling, leading to significantly enhanced scattering, as observed by Dark-field spectroscopy (Figure S19 and S20a). As mentioned above, the utilization of PDPACy3-III spacer (an approximate size ranging from 7.2 to 16.6 nm, Table S2) almost eliminated the influence of excitation enhancement as most of the dyes located in the center of gaps, where the enhancement ratio of the electric field is very close to 1 (Figure S21). Therefore, same as the clusters, the apparent

fluorescence intensity of vesicle was also dependent on a combined impact of quenching, intrinsic QY of Cy3, and scattering-induced enhancement. Theoretically, the formation of vesicle would lead to ~21.5-fold increase in Scat/(Scat+Abs) ratio (Figure 5e), which was accounted for the considerable increase of fluorescence enhancement ratio at pH 8.5 and 6. When vesicles disassembled into small clusters at a pH below its p*K*a (*i.e.,* pH 5 and 4), the fluorescence enhancement derived from strong scattering greatly reduced and thus resulted in a decreased enhancement ratio.

The vesicular structures retained their structural integrity at pH 8.5 and 6. Based on the simulation, the contribution of fluorescence intensity originating from the Scat/(Scat+Abs) ratios of vesicle at pH 8.5 and 6 was almost the same due to the similar morphology and physical size. The extending size of PDPA spacer when the pH decreased from 8.5 to 6 led to a less quenching effect for encoded Cy3 molecules, giving rise to an increased fluorescence intensity and thus a higher enhancement ratio. From pH 6 onwards, the large vesicle disassembled into small clusters (Figure 3c), leading to a significant reduction of Scat/(Scat+Abs) ratios. Therefore, at pH 5 and 4, the surface quenching again became a dominant effect, resulting in considerable decreases in fluorescence enhancement (Figure 4c). The experimental fluorescence enhancement ratios of the vesicles are between what are shown in curves 1, 3, and 2, 4 (Figure 5f). It suggested that the coexistence of the bilayer and interdigitated structures is present in the vesicular shell, but more likely to take the bilayer format. It should be noted that only 50 JNPs were taken into account for the simulation, which underestimated both scattering and fluorescence intensity of Cy3-encoded vesicles.

Importantly, the conjugation of PDPACy3-I on the Au/MFO led to significantly decayed QY,

which was only 5.1% compared to of the QY of free PDPACy3-I (Figure S22a). In the case of the vesicle, the apparent QY of JNP3 was 15% of free copolymer PDPACy3-III (Figure S22b). In combination with up to 6 times fluorescence enhancement of vesicle compared to that of the JNP3 building block, the vesicles collectively exhibited a brightness ~90% QY of the free PDPACY3-III. As a result, a bright fluorescent image was observed at pH 6 (Figure S20b). It demonstrated that the scattering-assisted enhancement was a considerable contribution to overall QY of the vesicle and was comparable to that of from quenching effect. In addition, incorporation of the magnetic MFO moiety endows a strong magnetic responsiveness to the vesicles, as observed in the hysteresis loop of Au/MFO JNP (Figure S23). Meanwhile, the time-lapse camera shows that the vesicles could be rapidly separated in a microfluidic chamber by an external magnetic field (100 Gauss) (Movie S1). The magnetic separation capability, together with plasmonic and fluorescent properties make Au/MFO-based vesicle a promising candidate for a multi-modality imaging application.

3 Conclusion

In summary, pH-triggered self-assembly of dye-conjugated polymer-coated magnetoplasmonic Au/MFO building blocks was conducted. By controlling the grafting density and the composition of polymers on the surface of Au/MFO, a morphological transition from cluster-to-lamellae-to-vesicle can be realized, which inherently is determined by the ratio of hydrophobic and hydrophilic polymer grafts on the Au/MFO. The self-assembly of amphiphilic Au/MFO leads to the formation of nanogaps between adjacent AuNPs and a larger cross-section associated with an increased Scat/(Scat+Abs) ratio. The use of well-defined

PDPACy3 BCP as grafts on AuNP allows to position the Cy3 molecules c in the interparticle gaps inside the assemblies, which make it possible to minimize the quenching effect due to the spacing function of the PDPA blocks. The nature of pH-responsiveness of PDPACy3 grafts also enables a pH-dependent control over the fluorescence intensity of corresponding assemblies and makes it an interesting platform to study the plasmon-fluorophore interaction. The combined experimental results and computational simulation demonstrated that the apparent fluorescence intensity of Cy3-encoded assemblies was primarily manipulated by surface quenching and scattering-induced enhancement, regardless of the electric field-related excitation enhancement. In the case of the cluster, quenching is the dominant effect due to the relatively close distance between Cy3 and AuNPs. The fluorescence intensity of the cluster is only 50% to that of its starting building block. For the vesicle, a decreasing quenching effect was achieved due to the utilization of higher M_w PDPACy3 spacer. In combination with the strong scattering derived from larger cross-section of the vesicle, the scattering-induced fluorescence enhancement is comparable to the decay of QY caused by surface quenching. Collectively, up to 6-folds fluorescence enhancement could be obtained in the vesicle. The findings bridge the structural parameters of dye-encoded plasmonic colloidal assemblies with their optical properties, and also provide a fundamental basis in designing plasmonic-fluorescent nanomaterials based on the MEF effect.

Acknowledgements

H.D. is grateful to the Ministry of Education Singapore for financial support (MOE2015-T2-1-112 and MOE2018-T2-2-128) and the authors thank Prof. Qihua Xiong for the assistance with fluorescence life-time characterization.

4 References

1. Kumar, A.; Kim, S.; Nam, J. M., Plasmonically Engineered Nanoprobes for Biomedical Applications. *J Am Chem Soc* **2016,** *138* (44), 14509-14525.
2. Lu, D.; Zhou, J.; Chen, Y.; Ma, J.; Duan, H., Self-Assembly of Polymer-Coated Plasmonic Nanocrystals: From Synthetic Approaches to Practical Applications. *Macromolecular rapid communications* **2019,** *40* (1), 1800613.
3. Lu, D.; Zhou, J.; Hou, S.; Xiong, Q.; Chen, Y.; Pu, K.; Ren, J.; Duan, H., Functional Macromolecule-Enabled Colloidal Synthesis: From Nanoparticle Engineering to Multifunctionality. *Advanced Materials* **2019,** *31* (44), 1902733.
4. Yi, C.; Yang, Y.; Liu, B.; He, J.; Nie, Z., Polymer-guided assembly of inorganic nanoparticles. *Chem Soc Rev* **2020**.
5. Cheng, L.; Liu, A. P.; Peng, S.; Duan, H. W., Responsive Plasmonic Assemblies of Amphiphilic Nanocrystals at Oil-Water Interfaces. *Acs Nano* **2010,** *4* (10), 6098-6104.
6. Cheng, L.; Song, J. B.; Yin, J.; Duan, H. W., Self-Assembled Plasmonic Dimers of Amphiphilic Gold Nanocrystals. *J Phys Chem Lett* **2011,** *2* (17), 2258-2262.
7. Song, J. B.; Wu, B. H.; Zhou, Z. J.; Zhu, G. Z.; Liu, Y. J.; Yang, Z.; Lin, L. S.; Yu, G. C.; Zhang, F. W.; Zhang, G. F.; Duan, H. W.; Stucky, G. D.; Chen, X. Y., Double-Layered Plasmonic-Magnetic Vesicles by Self-Assembly of Janus Amphiphilic Gold-Iron(II,III) Oxide Nanoparticles. *Angew Chem Int Edit* **2017,** *56* (28), 8110-8114.
8. Song, J. B.; Zhou, J. J.; Duan, H. W., Self-Assembled Plasmonic Vesicles of SERS-Encoded Amphiphilic Gold Nanoparticles for Cancer Cell Targeting and Traceable Intracellular Drug Delivery. *J Am Chem Soc* **2012,** *134* (32), 13458-13469.
9. He, J.; Liu, Y. J.; Babu, T.; Wei, Z. J.; Nie, Z. H., Self-Assembly of Inorganic Nanoparticle Vesicles and Tubules Driven by Tethered Linear Block Copolymers. *J Am Chem Soc* **2012,** *134* (28), 11342-11345.
10. He, J.; Huang, X. L.; Li, Y. C.; Liu, Y. J.; Babu, T.; Aronova, M. A.; Wang, S. J.; Lu, Z. Y.; Chen, X. Y.; Nie, Z. H., Self-Assembly of Amphiphilic Plasmonic Micelle-Like Nanoparticles in Selective Solvents. *J Am Chem Soc* **2013,** *135* (21), 7974-7984.
11. Song, J. B.; Huang, P.; Duan, H. W.; Chen, X. Y., Plasmonic Vesicles of Amphiphilic Nanocrystals: Optically Active Multifunctional Platform for Cancer Diagnosis and Therapy. *Accounts Chem Res* **2015,** *48* (9), 2506-2515.
12. Song, J. B.; Cheng, L.; Liu, A. P.; Yin, J.; Kuang, M.; Duan, H. W., Plasmonic Vesicles of Amphiphilic Gold Nanocrystals: Self-Assembly and External-Stimuli-Triggered Destruction. *J Am Chem Soc* **2011,** *133* (28), 10760-10763.
13. Liu, Y.; He, J.; Yang, K.; Yi, C.; Liu, Y.; Nie, L.; Khashab, N. M.; Chen, X.;

Nie, Z., Folding up of gold nanoparticle strings into plasmonic vesicles for enhanced photoacoustic imaging. *Angewandte Chemie International Edition* **2015,** *54* (52), 15809-15812.
14. Lim, D. K.; Jeon, K. S.; Hwang, J. H.; Kim, H.; Kwon, S.; Suh, Y. D.; Nam, J. M., Highly uniform and reproducible surface-enhanced Raman scattering from DNA-tailorable nanoparticles with 1-nm interior gap. *Nat Nanotechnol* **2011,** *6* (7), 452-460.
15. Nam, J. M.; Oh, J. W.; Lee, H.; Suh, Y. D., Plasmonic Nanogap-Enhanced Raman Scattering with Nanoparticles. *Accounts Chem Res* **2016,** *49* (12), 2746-2755.
16. Regmi, R.; Berthelot, J.; Winkler, P. M.; Mivelle, M.; Proust, J.; Bedu, F.; Ozerov, I.; Begou, T.; Lumeau, J.; Rigneault, H.; Garcia-Parajo, M. F.; Bidault, S.; Wenger, J.; Bonod, N., All-Dielectric Silicon Nanogap Antennas To Enhance the Fluorescence of Single Molecules. *Nano Lett* **2016,** *16* (8), 5143-5151.
17. Schmelzeisen, M.; Zhao, Y.; Klapper, M.; Mullen, K.; Kreiter, M., Fluorescence Enhancement from Individual Plasmonic Gap Resonances. *Acs Nano* **2010,** *4* (6), 3309-3317.
18. Chen, H.; Ming, T.; Zhao, L.; Wang, F.; Sun, L.-D.; Wang, J.; Yan, C.-H., Plasmon–molecule interactions. *Nano Today* **2010,** *5* (5), 494-505.
19. Yu, H.; Peng, Y.; Yang, Y.; Li, Z.-Y., Plasmon-enhanced light–matter interactions and applications. *npj Computational Materials* **2019,** *5* (1), 1-14.
20. Park, J. E.; Kim, J.; Nam, J. M., Emerging plasmonic nanostructures for controlling and enhancing photoluminescence. *Chem Sci* **2017,** *8* (7), 4696-4704.
21. Hou, S.; Chen, Y.; Lu, D.; Xiong, Q.; Lim, Y.; Duan, H., A Self-Assembled Plasmonic Substrate for Enhanced Fluorescence Resonance Energy Transfer. *Advanced Materials* **2020**, 1906475.
22. Ming, T.; Chen, H.; Jiang, R.; Li, Q.; Wang, J., Plasmon-controlled fluorescence: beyond the intensity enhancement. *The Journal of Physical Chemistry Letters* **2012,** *3* (2), 191-202.
23. Ayala-Orozco, C.; Liu, J. G.; Knight, M. W.; Wang, Y. M.; Day, J. K.; Nordlander, P.; Halas, N. J., Fluorescence Enhancement of Molecules Inside a Gold Nanomatryoshka. *Nano Lett* **2014,** *14* (5), 2926-2933.
24. Yang, J. J.; Faggiani, R.; Lalanne, P., Light emission in nanogaps: overcoming quenching. *Nanoscale Horiz* **2016,** *1* (1), 11-13.
25. Chang, W. S.; Willingham, B.; Slaughter, L. S.; Dominguez-Medina, S.; Swanglap, P.; Link, S., Radiative and Nonradiative Properties of Single Plasmonic Nanoparticles and Their Assemblies. *Accounts Chem Res* **2012,** *45* (11), 1936-1945.
26. Tam, F.; Goodrich, G. P.; Johnson, B. R.; Halas, N. J., Plasmonic enhancement of molecular fluorescence. *Nano Lett* **2007,** *7* (2), 496-501.
27. Pu, L.; Xu, J.; Sun, Y.; Fang, Z.; Chan-Park, M. B.; Duan, H., Cationic polycarbonate-grafted superparamagnetic nanoparticles with synergistic dual-modality antimicrobial activity. *Biomaterials science* **2016,** *4* (5), 871-879.
28. Sun, S. H.; Zeng, H.; Robinson, D. B.; Raoux, S.; Rice, P. M.; Wang, S. X.; Li, G. X., Monodisperse MFe2O4 (M = Fe, Co, Mn) nanoparticles. *J Am Chem Soc* **2004,** *126* (1), 273-279.
29. Zhou, K. J.; Liu, H. M.; Zhang, S. R.; Huang, X. N.; Wang, Y. G.; Huang, G.; Sumer, B. D.; Gao, J. M., Multicolored pH-Tunable and Activatable Fluorescence Nanoplatform Responsive to Physiologic pH Stimuli. *J Am Chem Soc* **2012,** *134* (18), 7803-

7811.
30. Zetterlund, P. B.; Thickett, S. C.; Perrier, S.; Bourgeat-Lami, E.; Lansalot, M., Controlled/living radical polymerization in dispersed systems: an update. *Chemical reviews* **2015,** *115* (18), 9745-9800.
31. Zhou, K. J.; Wang, Y. G.; Huang, X. N.; Luby-Phelps, K.; Sumer, B. D.; Gao, J. M., Tunable, Ultrasensitive pH-Responsive Nanoparticles Targeting Specific Endocytic Organelles in Living Cells. *Angew Chem Int Edit* **2011,** *50* (27), 6109-6114.
32. Mai, Y. Y.; Eisenberg, A., Self-assembly of block copolymers. *Chem Soc Rev* **2012,** *41* (18), 5969-5985.
33. Chandrawati, R.; Caruso, F., Biomimetic Liposome- and Polymersome-Based Multicompartmentalized Assemblies. *Langmuir* **2012,** *28* (39), 13798-13807.
34. Blanazs, A.; Madsen, J.; Battaglia, G.; Ryan, A. J.; Armes, S. P., Mechanistic Insights for Block Copolymer Morphologies: How Do Worms Form Vesicles? *J Am Chem Soc* **2011,** *133* (41), 16581-16587.
35. Matyjaszewski, K., Atom transfer radical polymerization (ATRP): current status and future perspectives. *Macromolecules* **2012,** *45* (10), 4015-4039.
36. Fielding, L. A.; Edmondson, S.; Armes, S. P., Synthesis of pH-responsive tertiary amine methacrylate polymer brushes and their response to acidic vapour. *J Mater Chem* **2011,** *21* (32), 11773-11780.
37. Zhou, J.; Xiong, Q.; Ma, J.; Ren, J.; Messersmith, P. B.; Chen, P.; Duan, H., Polydopamine-enabled approach toward tailored plasmonic nanogapped nanoparticles: from nanogap engineering to multifunctionality. *Acs Nano* **2016,** *10* (12), 11066-11075.
38. Acuna, G. P.; Bucher, M.; Stein, I. H.; Steinhauer, C.; Kuzyk, A.; Holzmeister, P.; Schreiber, R.; Moroz, A.; Stefani, F. D.; Liedl, T.; Simmel, F. C.; Tinnefeld, P., Distance Dependence of Single-Fluorophore Quenching by Gold Nanoparticles Studied on DNA Origami. *Acs Nano* **2012,** *6* (4), 3189-3195.
39. Seelig, J.; Leslie, K.; Renn, A.; Kuhn, S.; Jacobsen, V.; van de Corput, M.; Wyman, C.; Sandoghdar, V., Nanoparticle-induced fluorescence lifetime modification as nanoscopic ruler: Demonstration at the single molecule level. *Nano Lett* **2007,** *7* (3), 685-689.
40. Flory, P.; Mark, J.; Abe, A., Random-coil configurations of vinyl polymer chains. The influence of stereoregularity on the average dimensions. *J Am Chem Soc* **1966,** *88* (4), 639-650.
41. Yi, C.; Zhang, S.; Webb, K. T.; Nie, Z., Anisotropic self-assembly of hairy inorganic nanoparticles. *Accounts Chem Res* **2017,** *50* (1), 12-21.
42. Lu, D.; Hossain, M. D.; Jia, Z.; Monteiro, M. J., One-pot orthogonal copper-catalyzed synthesis and self-assembly of L-lysine-decorated polymeric dendrimers. *Macromolecules* **2015,** *48* (6), 1688-1702.
43. Tanabe, K., Field enhancement around metal nanoparticles and nanoshells: a systematic investigation. *The Journal of Physical Chemistry C* **2008,** *112* (40), 15721-15728.
44. Ming, T.; Chen, H. J.; Jiang, R. B.; Li, Q.; Wang, J. F., Plasmon-Controlled Fluorescence: Beyond the Intensity Enhancement. *J Phys Chem Lett* **2012,** *3* (2), 191-202.
45. Anderson, L. J. E.; Mayer, K. M.; Fraleigh, R. D.; Yang, Y.; Lee, S.; Hafner, J. H., Quantitative Measurements of Individual Gold Nanoparticle Scattering Cross Sections. *J Phys Chem C* **2010,** *114* (25), 11127-11132.

TOC graph

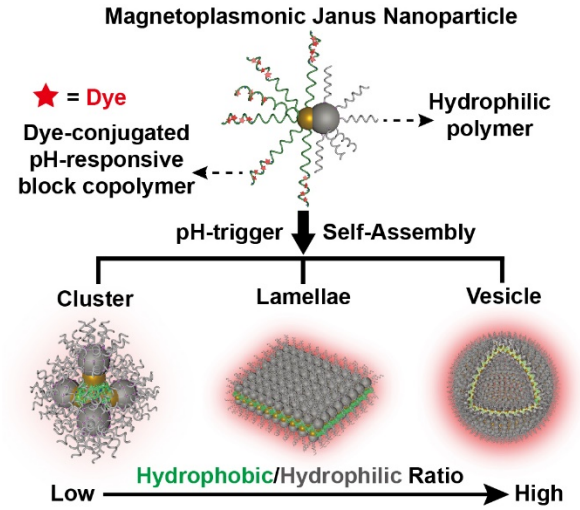
Magnetoplasmonic Janus Nanoparticle
= Dye
Dye-conjugated
pH-responsive
block copolymer
Hydrophilic
polymer
pH-trigger
Self-Assembly
Cluster
Lamellae
Vesicle
Hydrophobic/Hydrophilic Ratio
Low
High